Non-neural expression of SARS-CoV-2 entry genes in the olfactory epithelium suggests mechanisms underlying anosmia in COVID-19 patients

David Brann[*1], Tatsuya Tsukahara[*1], Caleb Weinreb[*1],
Darren W. Logan[2], Sandeep Robert Datta[1,3]

[1]Harvard Medical School Department of Neurobiology, Boston MA 02115 USA
[2]Waltham Petcare Science Institute, Leicestershire LE14 4RT, UK
[3]Corresponding Author

*These authors contributed equally to the manuscript

Abstract

Recent reports suggest an association between COVID-19 and altered olfactory function. Here we analyze bulk and single cell RNA-Seq datasets to identify cell types in the olfactory epithelium that express molecules that mediate infection by SARS-CoV-2 (CoV-2), the causal agent in COVID-19. We find in both mouse and human datasets that olfactory sensory neurons do not express two key genes required for CoV-2 entry, ACE2 and TMPRSS2. In contrast, olfactory epithelial support cells and stem cells express both of these genes, as do cells in the nasal respiratory epithelium. Taken together, these findings suggest possible mechanisms through which CoV-2 infection could lead to anosmia or other forms of olfactory dysfunction.

Introduction

SARS-CoV-2 (CoV-2) is a pandemic coronavirus that causes the COVID-19 syndrome, whose sequelae range from upper respiratory infection (URI) symptoms to severe respiratory distress, acute cardiac injury and death[1-4]. CoV-2 is closely related to other beta-coronaviruses, including the causal agents in pandemic SARS and MERS (SARS-CoV and MERS-CoV, respectively) and endemic viruses typically associated with mild URI syndromes (hCoV-OC43 and hCoV-299E)[5-7]. Anecdotal reports from clinicians and patients during the 2019-2020 pandemic suggest that infection with CoV-2 is associated with high rates of disturbances in smell and taste perception (anosmia, hyposmia, ageusia and/or dysgeusia)[8-11]. On March 20, 2020 the Ear, Nose, and Throat Society of the UK and the British Rhinological Society issued a bulletin detailing a strong anecdotal association between CoV-2 infection and anosmia/hyposmia in physician reports from South Korea, China, Italy, France and the United States; this bulletin further argued that individuals with new onset anosmia should self-isolate based upon presumed CoV-2 infection[12]. On March 22, 2020 the American Academy of Otolaryngology proposed that anosmia, hyposmia and dysgeusia (in the absence of other respiratory disease) should be added to symptoms used for screening for CoV-2 infection, and urged precautionary isolation for individuals with these symptoms[13].

A possible association between olfactory dysfunction and CoV-2 is consistent with a case report describing a patient with SARS with long term anosmia after recovery from respiratory distress[14], with the observation that olfactory function is commonly altered after infection with endemic coronaviruses[7,15-17], and with data demonstrating that intentional experimental infection of humans with hCoV-299E raises the thresholds at which odors can be detected[18]. Although definitive reports of widespread CoV-2-associated anosmia have not yet been published in the literature (but see[19]), these collective findings raise the question of how CoV-2 influences odor processing mechanisms to change smell perception in COVID-19 patients. While defects in olfaction may arise from changes in odor conduction associated with CoV-2-induced inflammation, it is also possible that CoV-2 infects and damages cells in the nasal epithelium required for normal olfactory function[15]. Addressing this question has important implications for the use of olfactory performance measures to support diagnosis and/or prognosis in COVID-19; furthermore, patients with persistent olfactory dysfunction are at risk of nutritional deficits, of injury due the inability to smell “danger” odors like smoke, gas and spoiled foods, and of developing psychiatric disorders, particularly depression [15,20-22].

The nasal epithelium is anatomically divided into two subdivisions, the respiratory epithelium (RE) and the sensory olfactory epithelium (OE), whose functions and cell types differ. In humans the vast majority of the nasal epithelium is RE (and correspondingly only a small portion is OE), whereas in rodents half of the nasal epithelium is OE[23,24]. The nasal RE is thought to humidify air as it enters the nose; main cell types include basal cells, ciliated cells, secretory cells (including goblet cells), and

brush/microvillar cells[24-26] (Fig. 1). The nasal RE is continuous with the epithelium that lines much of the respiratory tract, although transcriptional relationships between cell types observed in the nose RE and those found lower in the respiratory system remain unclear[24].

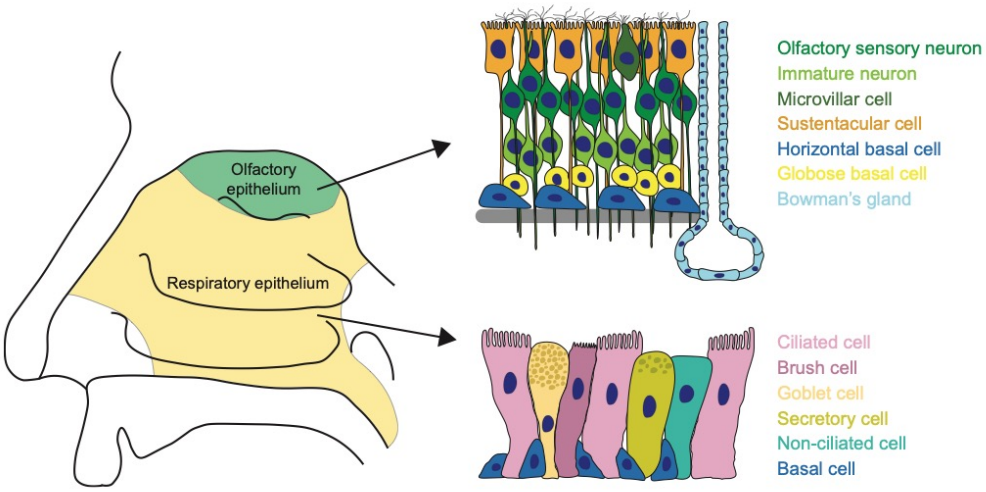

Figure 1. Schematic of nasal respiratory and olfactory epithelium.
Schematic of a sagittal view of the the human nasal cavity, in which respiratory and olfactory epithelium are colored (left). For each type of epithelium, a schematic of the anatomy and known major cell types are shown (right).

The OE is a laminated structure that houses a large number of mature olfactory sensory neurons (OSNs). These OSNs express odor receptors on their dendritic cilia, and their axons traverse the cribriform plate at the base of the skull to terminate in the olfactory bulb[27]. OSNs are therefore responsible both for detecting odors in the nasal airspace, and for transmitting information about odors to the brain. OSNs are supported by sustentacular cells, which have been proposed to act as structural supports for sensory neurons, to phagocytose and/or detoxify potentially damaging agents, and to maintain local salt and water balance[28-31] (Fig. 1). The OE contains several distinguishable types of basal stem cells that continuously renew sustentacular and OSN populations throughout life[32-34]. These stem cells include globose basal cells (GBCs), which are primarily responsible for regenerating OSNs during normal epithelial turnover, and horizontal basal cells (HBCs), which act as reserve stem cells activated upon tissue damage[35-37]. The OE also harbors additional cell types including microvillar cells (a subset of which may act as sensory cells), and mucus-secreting Bowman's gland cells[33,34].

CoV-2 — like SARS-CoV — infects cells through interactions between its spike (S) protein and the ACE2 protein on target cells; this interaction requires cleavage of the S protein by the cell surface protease TMPRSS2[4-6,38-42]. Thus ACE2 and TMPRSS2

are thought to be obligate for CoV-2 to infect cells, although proteases such as Cathepsin B and L (CTSB/CTSL) may also be involved[38]. Other coronaviruses use different cell surface molecules to facilitate cellular entry; these include DPP4 and FURIN for MERS-CoV, ANPEP for HCoV-299E, TMPRSS11D for SARS-CoV[43,44] (in addition to ACE2 and TMPRSS2), and ST6GAL1 and ST3GAL4 for HCoV-OC43 and HCoV-HKU1[6]. It has recently been demonstrated through single cell sequencing analysis (scSeq) that cells from the human upper airway — including nasal RE goblet, basal and ciliated cells —express high levels of ACE2 and TMPRSS2, suggesting that these RE cell types may serve as a viral reservoir during CoV-2 infection[45]. However, the analyzed samples did not include any OSNs or sustentacular cells, suggesting that tissue sampling in these experiments was limited to the RE and did not access the OE[46,47].

It therefore remains unclear whether any cell types in the OE express ACE2, TMPRSS2 or other molecules involved in coronavirus entry, which would render them susceptible to direct infection by CoV-2. To address the hypothesis that CoV-2 causes anosmia through primary effects on the OE, we queried publicly available mouse, non-human primate and human RNA sequencing (RNASeq) and scSeq datasets that include definitive OE populations to assess CoV-2-related gene expression[37,46,48-55]. We also mapped scSeq data across different datasets to compare observed gene expression levels from nasal samples to samples obtained from other airway tissues. Our results demonstrate that non-neural cells in the OE express CoV entry-associated molecules, suggesting that infection of these cells could directly or indirectly lead to olfactory dysfunction; this model potentially links gene expression patterns in olfactory support and stem cells to the clinical observation of anosmia in COVID-19 patients.

Results

To determine whether genes relevant to CoV entry are expressed in OSNs or other cell types in the olfactory mucosa, we examined published bulk RNA-Seq data sets obtained from the mouse. Several datasets were available in which sequencing was performed on the whole olfactory mucosa (WOM) and independently on purified populations of mature OSNs[51-53]. Reanalysis of the data from Saraiva et al.[52] showed that the CoV-2 receptor Ace2 and the protease Tmprss2 are expressed in WOM, as are the cathepsins Ctsb and Ctsl (Figure 2A). However, expression of these genes (with the exception of Ctsb) was much lower and Ace2 expression was virtually absent in purified OSN samples (mean ± SD normalized counts in OSNs; Ace2: 8.6 ± 4.2, Tmprss2 117.3 ± 24.7, Ctsb: 38616.7 ± 1650.2, Ctsl: 1705 ± 87; same in WOM; Ace2: 254.7 ± 22.5, Tmprss2 2279 ± 219.6, Ctsb: 22380 ± 947, Ctsl: 4900 ± 90.5, see Methods). These samples reflected the presence of expected cell types, as the WOM sequencing data included gene expression profiles associated with a wide variety of RE and OE cells, while the purified OSN samples were specifically enriched for markers of mature OSNs. The de-enrichment of Ace2 and Tmprss22 in OSNs relative to WOM was also observed in the two other mouse RNA-Seq datasets[51,53] (Figure 2B). We further probed these three mouse datasets to quantify the expression of genes involved in cell entry by other CoVs[6,38,45]. Except for St3gal4, all of these genes were detected in WOM and de-enriched in purified OSNs.

The presence of Ace2 and Tmprss2 transcripts in mouse WOM and their absence in purified OSNs suggest that the molecular components that enable CoV-2 entry into cells are largely expressed in non-neuronal cell types in the mouse nasal epithelium. To identify the specific cell types that express Ace2 and Tmprss2, we examined two recently published mouse OE scSeq datasets[49,50]. This analysis confirmed our results from bulk RNA-seq, as mature OSNs from either dataset did not express Ace2 (zero cells express Ace2 out of 5337 and 51 OSNs, respectively, Figures 2C, 2D). Ace2 was only detected in two cells (out of 8480) in the first dataset (which included cells drawn from mice aged P0 to P21[47]). However, Ace2 was detected in more than 1% of GBCs, more than 2% of HBCs and nearly 3% of sustentacular cells in the other dataset[37] (drawn from adult mice, Figure 2D). Furthermore, larger percentages of HBCs, GBCs and sustentacular cells expressed Tmprss2. Taken together, these bulk RNA-Seq and scSeq mouse data demonstrate that CoV-2 cell entry-related genes are expressed in the OE, and suggest that support and stem cells are the most likely candidates for CoV-2 infection within the OE.

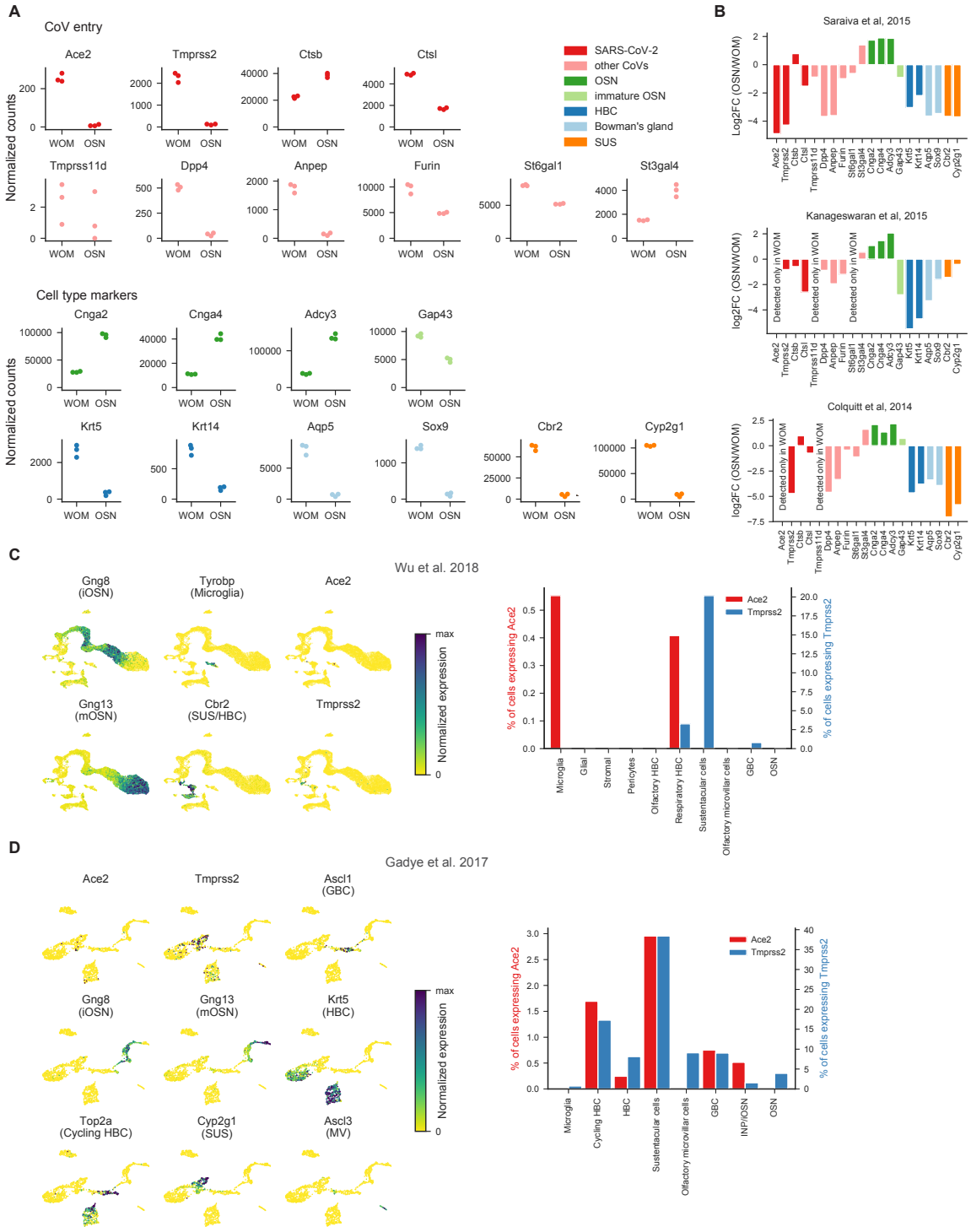

Figure 2. Coronavirus cell entry-related genes are expressed in mouse olfactory mucosa but not in mature OSNs. (A) Expression of coronavirus (CoV)-related genes and cell type markers in mouse olfactory mucosa in the data from Saraiva et al 2015[52]. Normalized counts for each gene in the whole olfactory mucosa (WOM) and olfactory sensory neurons (OSNs) are shown. Each circle represents a biological replicate and each color indicates the category of the gene shown on the right (SARS-CoV-2 and other CoVs: genes involved in the entry of these viruses, other categories: marker genes for specific

cell types such as horizontal basal cells (HBC), and sustentacular cells (SUS)). **(B)** Log_2-fold change (FC) of gene expression between OSNs and WOM, calculated for the genes shown in **A**. The mean expression level of each gene for each source dataset across replicates was used to calculate Log_2FC. Genes whose expression were detected only in WOM and not in OSNs are marked as 'Detected only in WOM'. **(C)** Expression of coronavirus (CoV) related genes and cell type markers in mouse scSeq data from Wu et al 2018[50]. Left, UMAP representation of single cell transcriptomes with normalized expression (nUMIs divided by the total counts for each cell) of marker genes for immature (Gng8) and mature (Gng13) OSNs. CoV related genes Ace2 and Tmprss2 are present in microglia (Tyrobp), and HBC/sustentacular cells (Cbr2). Each circle represents an individual cell, and the color represents the normalized expression level for each gene. Right, percent of cells expressing Ace2 and Tmprss2. Detection was considered positive if any transcripts (UMIs) were expressed for a given gene. Ace2 and Tmprss2 were not detected in any OSNs. **(D)** As in **A**, but in scSeq data from Gadye et al 2017[49]. Left, UMAP representation depicting normalized gene expression of maturing OSNs and non-neuronal cells. Neuronal cell types were identified by canonical markers for GBCs (Ascl1), immature OSNs (Gng8) and mature OSNs (Gng13). HBCs (Krt5) were categorized as quiescent or cycling on the basis of cell cycle markers (Top2a). Sustentacular cells (Cyp2g1) and microvillar cells (MV; Ascl3) were also identified. Right, percent of cells expressing Ace2 and Tmprss2 in each cell type. Sustentacular cells had the highest frequencies of expression for both Ace2 and Tmprss2. Ace2 was not detected in any OSNs.

To address whether similar patterns of gene expression were apparent in human samples, we took advantage of bulk WOM RNA-Seq data derived from macaque, marmoset and human. These datasets revealed expression of almost all CoV-entry-related genes in all WOM samples (Figure 3A). We therefore asked if, as in the mouse, human ACE2 is absent from OSNs but present in other OE cell types. To do so, we quantified expression of ACE2 and TMPRSS2 in scSeq derived from four human nasal biopsy samples recently reported by Durante et al[48]. Examination of human scSeq gene expression patterns and known marker genes distinguished OSNs, olfactory and respiratory HBCs, as well as subtypes of respiratory epithelial cells and other non-neuronal cells in the OE (Figure 3B-C). As in the mouse scSeq datasets, neither ACE2 nor TMPRSS2 were detected in mature OSNs, but these genes were detected in many sustentacular cells and HBCs (Figure 3D-F). Together, these results further support the notion that sustentacular and olfactory stem cells, but not mature OSNs, are the potential target of CoV-2 in the human OE.

We also sought to compare the frequency of ACE2 and TMPRSS2 expression between the cell types in the human RE and OE, as both types of epithelia were captured in the Durante et al. scSeq dataset[48]. Among mature cell types in the OE, sustentacular cells exhibited the highest frequency of ACE2 expression (2.9% of cells), as was observed in the mouse scSeq datasets; these frequencies were slightly lower than those observed in respiratory ciliated and secretory cells (3.7% and 3.9%, respectively). Although all HBC subtypes expressed ACE2, the frequency of expression of ACE2 was lower in olfactory HBCs (0.73% of cells) compared to respiratory HBCs (2.19% of cells) (Figure 3D).

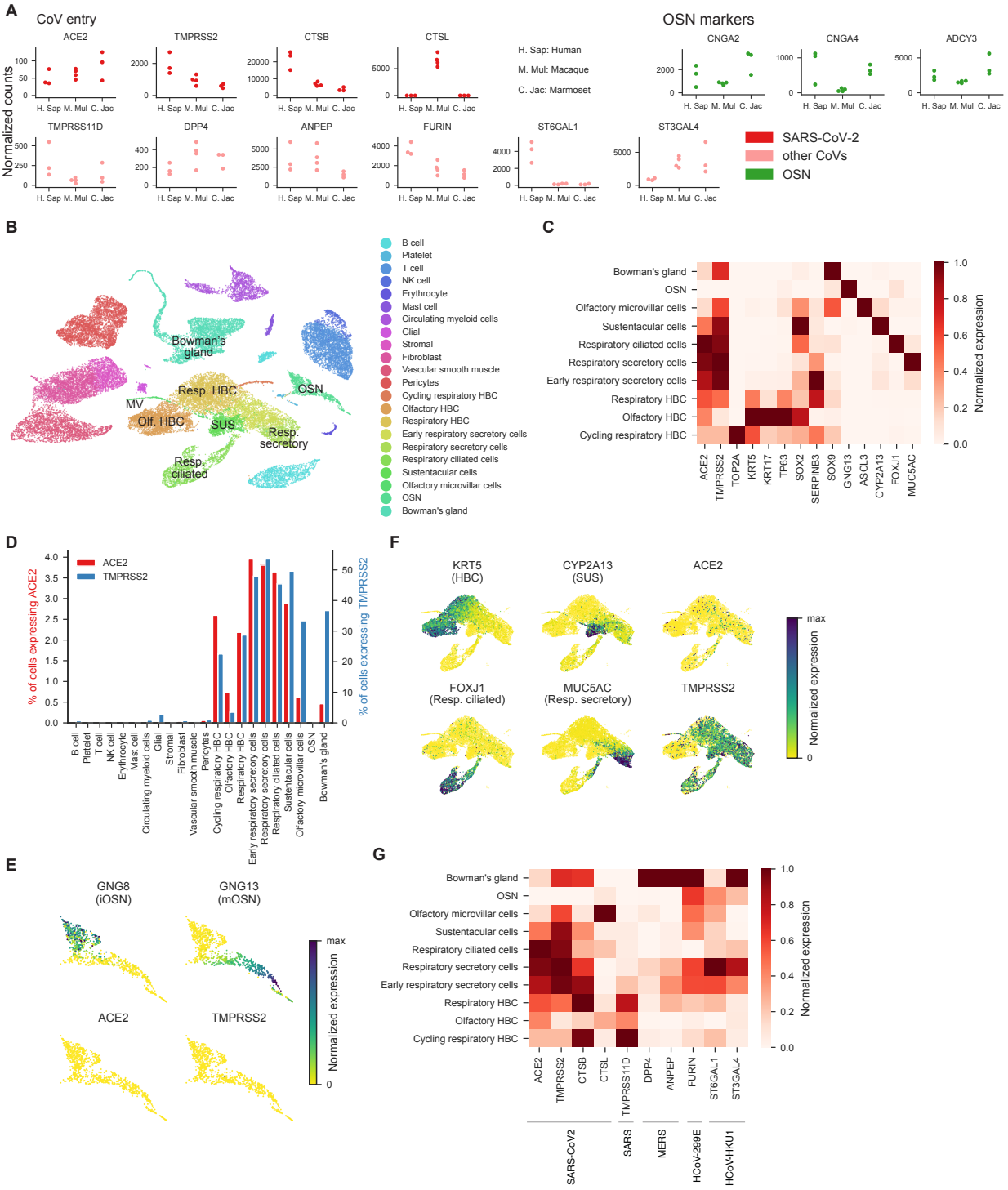

Figure 3. Coronavirus cell entry-related genes are expressed in human respiratory and olfactory epithelium, but are not detected in human OSNs. (A) Expression of genes required for the entry of coronavirus (CoV) and OSN markers in primate olfactory mucosa in the data from Saraiva et al 2019[54]. Human (H. Sap), Macaque (M. Mul) and Marmoset (C. Jal) data are shown. Each circle represents a biological replicate and each color indicates the category of the gene shown on the right. Raw counts were normalized to account for differences in sequencing depth between samples. **(B)** UMAP

representation of cell types in human nasal biopsy scSeq data from Durante et al. 2020[48]. Each dot represents an individual cell, colored by cell type. Several olfactory cell types shown in **C** are labeled in the plot, including OSNs, respiratory and olfactory HBCs, respiratory ciliated cells, sustentacular cells (SUS), microvillar cells (MV), and Bowman's gland cells. **(C)** Coronavirus related genes ACE2 and TMPRSS2 are expressed in respiratory and olfactory cell types, but not in OSNs. Gene expression for ACE2 and TMPRSS2 as well as marker genes for olfactory and respiratory epithelial subtypes are shown normalized by their maximum expression across cell types. **(D)** Percent of cells expressing ACE2 and TMPRSS2. ACE2 was not detected in any OSNs. **(E)** UMAP representations of 865 detected immature (GNG8) and mature (GNG13) OSNs. Neither ACE2 nor TMPRSS2 are detected in either population of OSNs. **(F)** UMAP representation of 10877 cells in the HBC lineages. ACE2 and TMPRSS2 are detected in HBC (KRT5) and sustentacular (CYP2A13) cells, as well as other respiratory epithelial cell types, including respiratory ciliated (FOXJ1) cells. TMPRSS2 was expressed less frequently in olfactory compared to respiratory HBCs (left population of KRT5 cells; see **3B**). **(G)** Gene expression, normalized as in **3C**, across olfactory and respiratory epithelial cell types for the entry of CoV-2 and other CoVs.

In addition, all other RE cell subtypes showed higher frequencies of ACE2 and TMPRSS2 expression than was apparent in OE cells. Although both microvillar cells and Bowman's gland cells (which reside in the OE) expressed TMPRSS2 at a frequency comparable to or higher than HBCs (33.12% and 36.71% versus 28.3%), they exhibited lower frequencies of ACE2 expression (0.63% and 0.46% versus 2.2%). While these results are consistent with sustentacular cells, microvillar cells, Bowman's gland cells and olfactory stem cells being susceptible to CoV-2 infection, CoV-2 may preferentially target RE cells based upon greater frequency of ACE2 and TMPRSS2 expression.

In addition to examining the expression patterns of ACE2 and TMPRSS2, we assessed the single-cell expression of genes involved in cell entry for other CoVs (Figure 3G). Although CTSB expression largely overlapped with that of ACE2 and TMPRSS2, other CoV entry-related genes were present in subsets of cell types, including OSNs, respiratory secretory and Bowman's gland cells. Few genes relevant to cell entry of other CoVs were expressed in sustentacular or olfactory HBCs; given the relative enrichment of ACE2 and TMPRSS2 in these cell types, this finding suggests that different CoVs may target distinct subsets of cells in the olfactory mucosa.

These results demonstrate the presence of key CoV-2 entry-related genes in specific cell types in the OE, but at lower levels of expression than in RE isolated from the nasal mucosa. We wondered whether these lower levels of expression might nonetheless be sufficient for infection of CoV-2. It was recently reported that nasal RE has higher expression of CoV-2 entry genes than RE of the trachea or lungs[45], and we therefore asked where OE fell within this previously established spectrum of expression. We took advantage of recently published data from Deprez and colleagues[46] in which biopsies of healthy human donors that spanned the nasal RE to the distal lung were subject to scSeq.

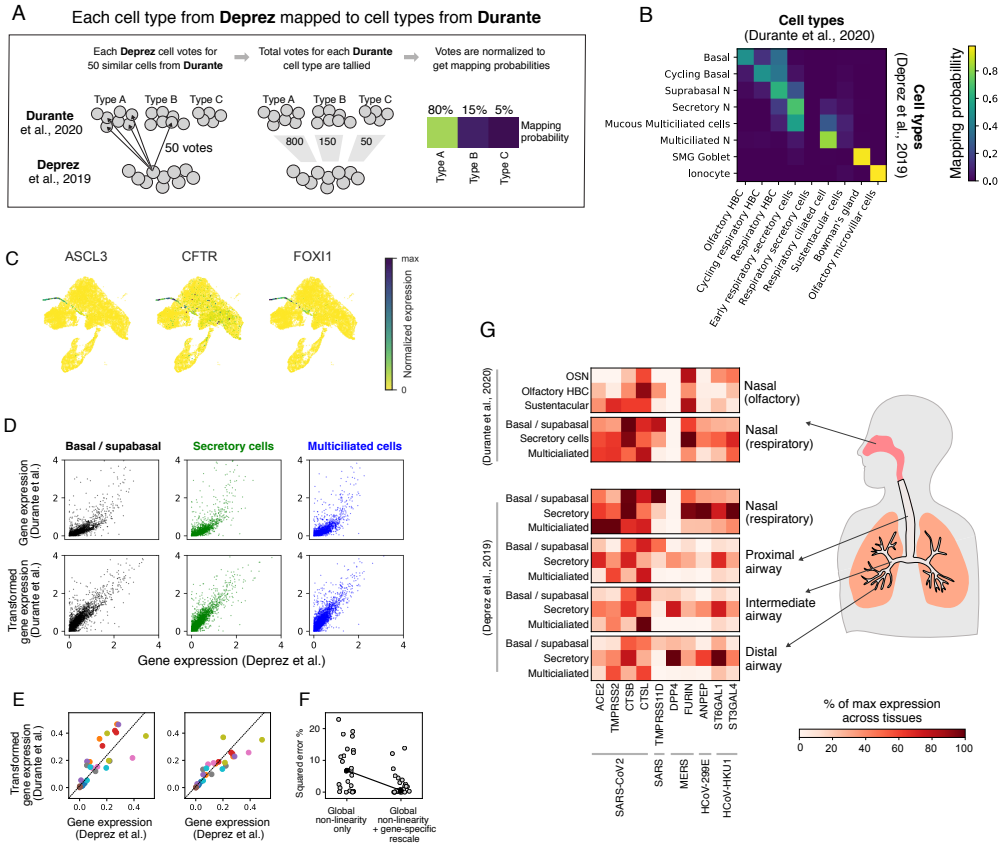

Figure 4. Comparing cell types and expression levels across respiratory and olfactory epithelial datasets. (A) Schematic of the mapping strategy used to identify similar cell types across datasets, applied to a toy example. Each cell type from the Deprez dataset was mapped to cell types from the Durante dataset. From left to right: Each Deprez cell voted on its 50 most similar cells in the Durante data; the total number of votes cast for each Durante cell type was quantified; and the vote totals were normalized to produce a set of mapping probabilities. **(B)** Similarity between cell types from the Durante et al. dataset and the Deprez et al. dataset. Heatmap indicates the mapping probability (see **A** and Methods). **(C)** Gene expression in olfactory microvillar cells from the Durante dataset. These cells express classical microvillar genes (ASCL3) as well as marker genes of pulmonary ionocytes (CFTR, FOXI1). **(D)** Top: average expression of for each gene in three cell types compared between the Durante and Deprez datasets in the units of the original papers. Bottom: average expression after a global non-linear transformation of the Durante data. Basal/suprabasal cells = “cycling respiratory HBCs” and “respiratory HBCs” from Durante et al., and “basal,” cycling basal,” and “suprabasal” cells from Deprez et al. Secretory cells = “early respiratory secretory cells” from Durante et al., and “secretory” cells from Deprez et al. Mutliciliated cells = “respiratory ciliated cells” from Durante et al., and “multiciliated” cells from Deprez et al. **(E)** Average expression of genes shown in **G** before (left) and after (right) gene-specific rescaling. Each color is one gene. For every color, three dots are shown, corresponding to expression across the three cell types in **D**. The diagonal line represents unity. Dots close to the diagonal line indicate a close match in transformed gene expression the Durante and Deprez data for the cell types shown in **D**. **(F)** Comparison of percent squared error before versus after gene-specific rescaling. **(G)** Gene expression across cell types and tissues in Durante et al. (top) and Deprez et al. (bottom). Each gene is normalized to its maximum value across all tissues. Gene expression from Durante et al was transformed (as in **D**-**E**; see Methods). The tissues correspond to progressive positions along the airway from nasal to distal lung.

To compare the gene expression levels in this respiratory dataset to those in the nasal mucosa-specific samples in the Durante et al dataset[48], we sought a mapping between cells in these two datasets to establish a common scale of gene expression. For each cell type in the Deprez lung dataset, a voting strategy was used to identify the most similar cell types in the Durante dataset: each Deprez cell 'voted' on the 50 most similar cells in the Durante dataset. The proportion of 'votes' belonging to each Durante cell type was recorded, and these proportions were reported as the "mapping probabilities" shown in Figure 4 (see Methods). The resulting map of cell type similarity (Figure 4B) revealed a correspondence between the RE cell types in each dataset, including HBCs, multiciliated cells and secretory cells. Two strong associations were also detected between RE and OE cell types: goblet cells in the RE were similar to Bowman's cells in the OE (96% mapping probability, see Methods) and pulmonary ionocytes in the RE were similar to microvillar cells in the OE (99% mapping probability, see Methods). Pulmonary ionocytes are a recently characterized cell type in the lung RE that express CFTR proteins and the transcription factor FOXI1, which specifies ionocyte cell fate and regulates expression of V-ATPase subunits that participate in ion exchange[56]. Microvillar cells in the Durante dataset exhibited similar high-level expression of CFTR and FOXI1 (Figure 4C); however, these cells did not express other markers of microvillar cells (such as TRPM5, IP3R3 and CD73), suggesting that they are either immature microvillar cells or a distinct microvillar subtype residing in the nasal mucosa[57].

To match gene expression values across the Durante and Deprez datasets, we developed a fitting procedure to transform gene expression levels such that they were equal for cell types common to both datasets (Figures 4D-F). This approach — which involved a global non-linearity to account for the different normalization methods used on each dataset, followed by a gene-specific rescaling to account for differences in gene capture techniques — revealed that ACE2 and TMPRSS2 expression in human OE sustentacular cells was on par with expression of these genes in the remainder of the non-nasal respiratory tract (Figure 4G)[45].

Discussion

Here we demonstrate that subsets of sustentacular cells, Bowman's gland cells and HBCs in the OE co-express the CoV-2 receptor ACE2 and the spike protein protease TMPRSS2. OE sustentacular cells express these genes at levels comparable to that observed in lung cells. However, in all queried mouse and human RNA-Seq and scSeq datasets, ACE2 and TMPRSS2 are not expressed in mature OSNs. These observations suggest that CoV-2 does not directly enter OSNs, but instead may target OE support and stem cells. Infection of these non-neural cell types — rather than infection of sensory neurons — may therefore be responsible for anosmia and related disturbances in odor perception in COVID-19 patients.

Many possible mechanisms have been proposed through which viruses can alter olfactory function, including inflammation-related deficits in odor conduction and primary damage to the olfactory epithelium[15,16]. Viral injury has been extensively modeled in rodents, which has revealed substantial diversity among viruses (and even within different types of coronaviruses) in the nature and extent of damage to the OE[16,58-61]. Intriguingly, infection of the rat with the SDAV coronavirus appears to cause denuding of ciliary cells in the RE, reduction in the number of goblet cells in the RE, and focal infection of subsets of sustentacular cells in the OE. SDAV infection follows a characteristic trajectory, with substantial RE infection preceding OE infection by several days[58]. This pattern is precisely what one might predict for CoV-2 infection in humans, given the cell types that express ACE2 and TMPRSS2 in the peripheral olfactory system. Importantly, despite the fact that infection in the OE appears limited to small numbers of sustentacular cells, as SDAV infection proceeds OSNs become denuded of cilia (presumably foreclosing the possibility of odor transduction) followed by a disruption in the global architecture of the OE[58]. These observations suggest that coronavirus infection of subsets of sustentacular cells may be sufficient to cause cascading damage in the OE that culminates in the disruption of OSN function.

It is also possible that infection of stem cells such as HBCs — which express ACE2 and TMPRSS2 at lower levels than RE or sustentacular cells — contributes to olfactory dysfunction. The survival time of mature OSNs varies based upon many factors, but on average in the mouse such neurons survive weeks to short months, rather than days or years[62,63]. Although HBCs in mice appear largely quiescent, recent human scSeq data suggests that ongoing neurogenesis may play a larger role than previously appreciated in the human OE[48]. It is therefore possible, over the timescale of CoV2 infection, that damage to HBCs plays a causal role in the development of anosmia; given the slow rate of turnover apparent in OSNs, a more likely scenario is that the dual challenge to the OE of acute loss of sustentacular cells, taken with the inability to effectively renew the OE over time, may result in long-lasting anosmia. Furthermore, work in mice suggests that injury can cause de-differentiation of neuronal progenitors, which may suppress ongoing neurogenesis and potentially abrogate olfactory function.[64]

ACE2 and TMPRSS2 were also expressed in microvillar and Bowman's gland cells in the OE. Our analysis mapping cells in the nasal RE and OE to cells in the lower respiratory system suggest that the nasal mucosa microvillar cells in the Durante dataset are related to previously identified pulmonary ionocytes[56]. As ionocytes are critical determinants of local ion balance in the lung, damage to closely-related microvillar cells in the OE could potentially alter ion gradients and hence firing properties of sensory neurons. Damage to Bowman's gland cells may also contribute to olfactory dysfunction, as lesions of this cell type have been linked to broad disruption of the olfactory neuroepithelium[65].

Given that the natural history of CoV2-induced anosmia is only now being defined, and no causal experiments have yet been done in model organisms exploring CoV-2 infection of the OE, it remains unclear whether sustentacular cells, HBCs, microvillar cells, Bowman's gland cells or some cells of an as-yet-unidentified type are the key olfactory pathophysiological targets for CoV-2. The importance of secondary inflammatory processes also remains to be assessed. It further remains unclear whether the effects of CoV-2 on smell are responsible for changes in taste perception, or whether taste is affected by independent mechanisms. One clear caveat of our analysis is that scSeq is subject to well-known sampling artifacts related to cell type composition and gene expression capture. These biases may account for the observation that ACE2 and TMPRSS2 are only modestly expressed in OE cells; however, we favor the alternative possibility that these genes are expressed in limited subsets of the overall population. Consistent with this notion, a previous microarray-based analysis of gene expression in bulk sorted mouse sustentacular cells[66] did not reveal an enrichment of ACE2 expression with respect to other cell types (data not shown).

The datasets explored herein are limited to the nasal mucosa and respiratory tract. However, viral-induced deficits in olfactory function may also be caused by central dysfunction in higher-order olfactory structures. Many viruses, including coronaviruses, have been shown to propagate from the nasal epithelium past the cribriform plate to infect the olfactory bulb and downstream areas like piriform cortex; this form of central infection has been suggested to mediate olfactory deficits, even in the absence of lasting OE damage[16,40,59,61,67-69]. Coronoviral RNA has been identified in the brains of patients, suggesting this possibility as a pathophysiological mechanism in the case of COVID-19[67,70]. That said, it remains unclear whether or how CoV-2 might infect or influence central olfactory structures, given that CoV-2 is unlikely to directly infect the OSNs that send axons to the brain. The rodent coronavirus MHV has been shown to pass from the nose to the bulb, but OSNs do not express CEACAM1, the main MHV receptor[59,71] (data not shown); this observation suggests that coronavirus in the nasal mucosa may reach the brain through mechanisms independent of axonal transport by sensory nerves. Exploring this possibility is an important avenue for future CoV-2-related olfactory research.

One interesting feature revealed in our analysis is that mouse and human OSNs express several molecules relevant to cell entry of other CoVs, including FURIN, ST6GAL1 and ST3GAL4. This finding suggests mechanisms through which other CoVs could infect primary OSNs. We also observed lower levels of ACE2 and TMPRSS2 expression in RE and OE cells from juvenile mice, in contrast to the higher levels observed in scSeq from adult humans. Although both negative and cross-species data should be interpreted with extreme caution, if younger humans (like their mouse counterparts) also express relatively low levels of ACE2 and TMPRSS2, then young COVID-19 patients may be less susceptible to CoV-2-mediated olfactory damage. Furthermore, if the recently-proposed hypothesis that RE cells act as a reservoir of CoV-2 is found to be true[45], then a highly speculative possibility is that differences in expression of ACE2 and TMPRSS2 in the nasal epithelium (or upper airways) may in part explain the milder clinical course for COVID-19 observed in younger patients. Further scSeq experiments in adult mice and juvenile humans will be required to definitively characterize differences in ACE2 and TMPRSS2 expression over time.

Acknowledgements

We thank members of the Datta lab, James Schwob, John Ngai, Bernardo Sabatini, Andreas Schaefer, Kevin Franks, Michael Greenberg and Vanessa Ruta for helpful comments on the manuscript. SRD is supported by grants RO11DC016222 and U19 NS112953 from the National Institutes of Health and by the Simons Collaboration on the Global Brain.

Methods

Mouse bulk RNA-Seq datasets

Normalized gene expression tables were obtained from previous published datasets[51-54]. For the mouse data sets, the means of the replicates from WOM or OSN were used to calculate Log_2 fold changes. For the mouse data from Saraiva et al. and the primate data sets[52,54], the normalized counts of the genes of interest from individual replicates were plotted. Below is a table for the detailed sample information.

Sample information for the bulk RNA-seq data analyzed in this study

	source	species	reps	samples per rep	Sex (M/F)	age	strain	Geno
Saraiva et al., 2015	WOM	mouse	3	1	2/1	P21	OMP-IRES-GFP	GFP/+
	OSN	mouse	3	14–16	mixed	P25	OMP-IRES-GFP	GFP/+
Kanageswaran et al., 2015	WOM	mouse	4	3	F	4 wks	C57BL/6J	WT
	OSN	mouse	2	6-8	mixed	adult	OMP-IRES-GFP	GFP/+ or GFP/GFP
Colquitt et al, 2014	WOM	mouse	2	n.s.	n.s.	3 wks	Dnmt3a	WT
	OSN	mouse	2	n.s.	n.s.	3 wks	Dnmt3a	WT
Saraiva et al., 2019	WOM	Human	3	1	3/0	n.s.	NA	
	WOM	Macaque	3	1	n.s.	~4.5 yr.	NA	
	WOM	Marmoset	3	1	n.s.	~1-10 yr.	NA	

n.s., not specified

Mouse scSeq datasets

Single-cell RNA-seq data from Wu et al.[50] were downloaded from the Gene Expression Omnibus (GEO) at accession GSE120199. These data consisted of dissociated cells from the mouse olfactory epithelium from four developmental time points (P0, P3, P7, P21). The four datasets were aggregated and processed for visualization using the SPRING pipeline[72]. Briefly: total counts were normalized to the median total counts for each cell and highly variable genes selected using the SPRING gene filtering function ("filter_genes") using parameters (90 ,3, 3). Putative doublet cells were removed using Scrublet (8% of cells removed)[73]. Prior to two-dimensional visualization, the dimensionality of the data was reduced to 40 using principal components analysis (PCA). PCA-batch-correction, as described,[74] was applied to combine time points using P21 as a reference set. A batch balanced K-nearest neighbor graph was constructed using the top 20 principal components and the cells from this neighbor graph were visualized in two dimensions using UMAP with parameters min_dist: 0.5, n_epoch: 500, and learning_rate: 0.5[75]. Cell type annotation was performed manually using the following marker genes: OSNs (Gng8, Gng13), Microglia/Macrophages (Tyrobp, Trem2), Respiratory HBC (Krt5 and absence of Cxcl14), Olfactory HBC (Krt5 and Cxcl14), GBC (Sox11, Top2a), Glial (Fabp7, Plp1),

Olfactory microvillar cell (Ascl3), Pericyte/endothelial (Kdr, Tie1), Stromal (Lum, Myl9), Sustentacular (Cyp2a5, Cyp2g1).

The filtered dataset from the MOE contained 8480 cells with at least 1.3k cells from each time point. Each of the identified cell types also contained cells from each time point. Expression of candidate CoV-2-related genes was defined if at least one transcript (UMI) was detected in that cell, and the percent of cells expressing candidate genes was calculated for each cell type. Of the 5337 OSNs identified, none of them expressed Ace2 and only 5 cells (0.09 %) expressed Tmprss2. Although Ace2 was only detected in 2 cells total, Tmprss2 was detected in nearly 20% of sustentacular cells, as well as 3% of respiratory HBCs.

Single-cell RNA-seq data from HBC-derived cells from Fletcher et al. and Gadye et al[37,49], labeled via *Krt5-CreER* driver mice, were downloaded from GEO at accession GSE99251 using the file "GSE95601_oeHBCdiff_Cufflinks_eSet_counts_table.txt.gz". Processing was performed as described above, including total counts normalization and filtering for highly variable genes using the SPRING gene filtering function "filter_genes" with parameters (75, 20, 10). The resulting data were visualized in SPRING and a subset of cells were removed for quality control, including a cluster of cells with low total counts and another with predominantly reads from ERCC spike-in controls. Putative doublets were also identified using Scrublet and removed (6% of cells). The resulting data were visualized in SPRING and partitioned using Louvain clustering on the SPRING k-nearest-neighbor graph using the top 40 principal components. Cell type annotation was performed manually using the same set of markers genes listed above. Three clusters were removed for quality control, including one with low total counts and one with predominantly reads from ERCC spike-in controls (likely background), and one with high mitochondrial counts (likely stressed cells). For visualization, the remaining cells were projected to 20 dimensions using PCA and visualized with UMAP using the parameters described above.

The filtered dataset of mouse HBC-derived cells contained 1450 cells with at least 1.3k cells from each time point. The percent of cells expressing each marker gene was calculated as described above. Of the 51 OSNs identified, none of them expressed Ace2, and only 1 out of 194 immature OSNs expressed Ace2. In contrast, Ace2 and Tmprss2 were both detected in HBCs and sustentacular cells.

Human nasal scSeq dataset

Human scSeq data from Durante et al.[48] was downloaded from the GEO at accession GSE139522. 10X Genomics mtx files were filtered to remove any cells with fewer than 500 total counts. Additional preprocessing was performed as described above, including total counts normalization and filtering for highly variable genes using the SPRING gene filtering function "filter_genes" with parameters (90, 3, 10). The resulting data were visualized in SPRING and partitioned using Louvain clustering on the SPRING k-nearest-neighbor graph. Four clusters were removed for quality control,

including two with low total counts (likely background) and two with high mitochondrial counts (likely stressed or dying cells). Putative doublets were also identified using Scrublet and removed (7% of cells). The remaining cells were projected to 40 dimensions using PCA. PCA-batch-correction was performed using Patient 4 as a reference. The filtered data were then re-partitioned using Louvain clustering on the SPRING graph and each cluster was annotated using known marker genes, as described in[48]. For example, immature and mature OSNs were identified via their expression of GNG8 and GNG13, respectively. HBCs were identified via the expression of KRT5 and TP63 and olfactory HBCs were distinguished from respiratory HBCs via the expression of CXCL14 and MEG3. Identification of sustentacular (CYP2A13, CYP2J2), Bowman's gland (SOX9, GPX3), and olfactory microvillar cells (ASCL3, FOXI1) was also performed using known marker genes. For visualization, the top 25 principal components were reduced to two dimensions using UMAP with the parameters described above.

The filtered human scSeq dataset contained 33358 cells. Each of the patients contained cells from both the olfactory and respiratory epithelium, although the frequency of OSNs and respiratory cells varied across patients, as previously described[48]. 295 cells expressed ACE2 and 4953 cells expressed TMPRSS2. The percent of cells expression each ACE2 and TMPRSS2 was calculated for each cell type. Of the 865 identified OSNs, including both immature and mature cells, none of the cells express ACE2 and only 2 (0.23%) expressed TMPRSS2. In contrast, ACE2 was reliably detected in at least 2% and TMPRSS2 was expressed in close to 50% of multiple respiratory epithelial subtypes. The expression of both known cell type markers and known CoV-related genes was also examined across respiratory and olfactory epithelial cell types. For these gene sets, the mean expression in each cell type was calculated and normalized by the maximum across cell types.

Mapping scSeq datasets to each other

Data from Deprez et al.[46] were downloaded from the European Genome-phenome Archive at accession EGAS00001004082. A subset of these data was combined with a subset of the Durante data for mapping between cell types. For the Deprez data, the subset consisted of samples from the nasal RE that belonged to a cell type with >20 cells, including Basal, Cycling Basal, Suprabasal N, Secretory N, Mucous Multiciliated cells, Multiciliated N, SMS Goblet, Ionocyte. For the Durante data, the subset consisted of cells from cell types that had some putative similarity to cells in the Deprez dataset, including Olfactory HBC, Cycling respiratory HBC, Respiratory HBC, Early respiratory secretory cells, Respiratory secretory cells, Sustentacular cells, Bowman's gland, Olfactory microvillar cells.

To establish a cell type mapping:

1) Durante[48] and Deprez[46] data were combined and total counts normalized so that all cells across datasets had the same total counts. PCA was then performed

using highly variable genes and PCA-batch-correction with the Deprez data as a reference set.

2) Each cell from the Deprez data then 'voted' for the 50 most similar cells in the Durante data. A table *T* counting votes across cell types was then computed, where for cell type *i* in the Deprez data and cell type *j* in the Durante data,

$$T_{ij} = \{\text{number of votes cast from cells of type } i \text{ to cells of type } j\}$$

Thus, if the Deprez dataset has *N* cells, then *T* would count 50*N votes ($\sum T_{ij} = 50N$)

3) The table of votes *T* was normalized, resulting in a table of mapping probabilities *P*, which is shown in Fig 4B. Specifically:

$$P_{ij} = \frac{T_{ij}}{\sum_j T_{ij}}$$

Based on the table of mapping probabilities, we determined the following set of cell type correspondences for downstream analysis: Basal/suprabasal cells = "cycling respiratory HBCs" and "respiratory HBCs" from Durante et al., and "basal," cycling basal," and "suprabasal" cells from Deprez et al. Secretory cells = "early respiratory secretory cells" from Durante et al., and "secretory" cells from Deprez et al. Mutliciliated cells = "respiratory ciliated cells" from Durante et al., and "multiciliated" cells from Deprez et al.

We next sought a transformation of the Durante data so that it would agree with the Deprez data within the corresponding cell types identified above. To account for differing normalization strategies applied to each dataset prior to download (log normalization for Deprez et al. but not for Durante et al.), we used the following ansatz for the tranformation, where the pseudocount *p* is a global latent parameter and the rescaling factors f_i are fit to each gene separately. In the equation below, *T* denotes the transformation and e_{ij} represents a gene expression value for cell *i* and gene *j* in the Durante data:

$$T(e_{ij}) = \big(\log(e_{ij} + p) - \log(p)\big)/f_j$$

The parameter *p* was fit by maximizing the correlation of average gene expression across all genes between each of the cell type correspondences listed above. The rescaling factors f_i were then fitted separately for each gene by taking the quotient of average gene expression between the Deprez data and the log-transformed Durante data, again across the cell type correspondences above.

References

1 Guan, W.-j. *et al.* Clinical Characteristics of Coronavirus Disease 2019 in China. *N. Engl. J. Med.* **EPub ahead of print**, doi:10.1056/NEJMoa2002032 (2020).

2 Rothan, H. A. & Byrareddy, S. N. The epidemiology and pathogenesis of coronavirus disease (COVID-19) outbreak. *J. Autoimmun.* **EPub ahead of print**, doi:10.1016/j.jaut.2020.102433 (2020).

3 Wu, Z. & McGoogan, J. M. Characteristics of and Important Lessons From the Coronavirus Disease 2019 (COVID-19) Outbreak in China: Summary of a Report of 72 314 Cases From the Chinese Center for Disease Control and Prevention. *JAMA* **EPub ahead of print**, doi:10.1001/jama.2020.2648 (2020).

4 Zhou, P. *et al.* A pneumonia outbreak associated with a new coronavirus of probable bat origin. *Nature* **579**, 270-273, doi:10.1038/s41586-020-2012-7 (2020).

5 Ceccarelli, M., Berretta, M., Venanzi Rullo, E., Nunnari, G. & Cacopardo, B. Differences and similarities between Severe Acute Respiratory Syndrome (SARS)-CoronaVirus (CoV) and SARS-CoV-2. Would a rose by another name smell as sweet? *Eur Rev Med Pharmacol Sci* **24**, 2781-2783, doi:10.26355/eurrev_202003_20551 (2020).

6 Zumla, A., Chan, J. F. W., Azhar, E. I., Hui, D. S. C. & Yuen, K.-Y. Coronaviruses - drug discovery and therapeutic options. *Nat Rev Drug Discov* **15**, 327-347, doi:10.1038/nrd.2015.37 (2016).

7 Corman, V. M., Muth, D., Niemeyer, D. & Drosten, C. Hosts and Sources of Endemic Human Coronaviruses. *Adv. Virus Res.* **100**, 163-188, doi:10.1016/bs.aivir.2018.01.001 (2018).

8 Bienkov, A. *If you've lost your sense of smell or taste, you could be a 'hidden carrier' of the coronavirus*, <https://www.businessinsider.com/coronavirus-symptoms-loss-of-smell-taste-covid-19-anosmia-hyposmia-2020-3> (2020).

9 Gale, J. *NBA Player's Loss of Smell Highlights Unusual Marker of Covid-19*, <https://www.bloomberg.com/news/articles/2020-03-23/nba-player-s-loss-of-smell-highlights-unusual-marker-of-covid-19?utm_campaign=news&utm_medium=bd&utm_source=applenews> (2020).

10 Rabin, R. *Loss of sense of smell may be peculiar clue to coronavirus infection*, <https://www.nytimes.com/2020/03/22/health/coronavirus-symptoms-smell-taste.html> (2020).

11 Stone, J. *There's An Unexpected Loss Of Smell And Taste In Coronavirus Patients*, <https://www.forbes.com/sites/judystone/2020/03/20/theres-an-unexpected-loss-of-smell-and-taste-in-coronavirus-patients/#714e8b6a5101> (2020).

12 Hopkins, C. & Kumar, N. *Loss of sense of smell as marker of COVID-19 infection*, <https://www.entuk.org/sites/default/files/files/Loss%20of%20sense%20of%20smell%20as%20marker%20of%20COVID.pdf> (2020).

13 *Anosmia, Hyposmia, and Dysgeusia Symptoms of Coronavirus Disease*, <https://www.entnet.org/content/coronavirus-disease-2019-resources> (2020).
14 Hwang, C.-S. Olfactory neuropathy in severe acute respiratory syndrome: report of A case. *Acta Neurol Taiwan* **15**, 26-28, doi: uuid/B05A7D42-9FC0-46A4-8483-D0FE90434E53 (2006).
15 Dalton, P. Olfaction and anosmia in rhinosinusitis. *Curr Allergy Asthma Rep* **4**, 230-236, doi:10.1007/s11882-004-0031-3 (2004).
16 Doty, R. L. Systemic diseases and disorders. *Handb Clin Neurol* **164**, 361-387, doi:10.1016/B978-0-444-63855-7.00021-6 (2019).
17 Suzuki, M. *et al.* Identification of viruses in patients with postviral olfactory dysfunction. *Laryngoscope* **117**, 272-277, doi:10.1097/01.mlg.0000249922.37381.1e (2007).
18 Åkerlund, A., Bende, M. & Murphy, C. Olfactory threshold and nasal mucosal changes in experimentally induced common cold. *Acta Otolaryngol.* **115**, 88-92, doi:10.3109/00016489509133353 (1995).
19 Mao, L. *et al.* Neurological Manifestations of Hospitalized Patients with COVID-19 in Wuhan, China: a retrospective case series study. *medRxiv*, 1-26, doi:10.1101/2020.02.22.20026500 (2020).
20 Croy, I., Nordin, S. & Hummel, T. Olfactory disorders and quality of life--an updated review. *Chemical Senses* **39**, 185-194, doi:10.1093/chemse/bjt072 (2014).
21 Kohli, P., Soler, Z. M., Nguyen, S. A., Muus, J. S. & Schlosser, R. J. The Association Between Olfaction and Depression: A Systematic Review. *Chemical Senses* **41**, 479-486, doi:10.1093/chemse/bjw061 (2016).
22 Yuan, T.-F. & Slotnick, B. M. Roles of olfactory system dysfunction in depression. *Prog. Neuropsychopharmacol. Biol. Psychiatry* **54**, 26-30, doi:10.1016/j.pnpbp.2014.05.013 (2014).
23 Harkema, J. R., Carey, S. A. & Wagner, J. G. The nose revisited: a brief review of the comparative structure, function, and toxicologic pathology of the nasal epithelium. *Toxicol Pathol* **34**, 252-269, doi:10.1080/01926230600713475 (2006).
24 Reznik, G. K. Comparative anatomy, physiology, and function of the upper respiratory tract. *Environ Health Perspect* **85**, 171-176, doi:10.1289/ehp.85-1568330 (1990).
25 Hedrich, H. J. *The Laboratory Mouse*. (Academic Press, 2012).
26 Mery, S., Gross, E. A., Joyner, D. R., Godo, M. & Morgan, K. T. Nasal diagrams: a tool for recording the distribution of nasal lesions in rats and mice. *Toxicol Pathol* **22**, 353-372, doi:10.1177/019262339402200402 (1994).
27 Axel, R. The molecular logic of smell. *Scientific American* **273**, 154-159 (1995).
28 Pixley, S. K., Farbman, A. I. & Menco, B. P. Monoclonal antibody marker for olfactory sustentacular cell microvilli. *Anat Rec* **248**, 307-321, doi:(null) (1997).
29 Suzuki, Y., Schafer, J. & Farbman, A. I. Phagocytic cells in the rat olfactory epithelium after bulbectomy. *Exp. Neurol.* **136**, 225-233, doi:10.1006/exnr.1995.1099 (1995).
30 Suzuki, Y., Takeda, M. & Farbman, A. I. Supporting cells as phagocytes in the olfactory epithelium after bulbectomy. *J. Comp. Neurol.* **376**, 509-517, doi:(null) (1996).
31 Vogalis, F., Hegg, C. C. & Lucero, M. T. Ionic conductances in sustentacular cells of the mouse olfactory epithelium. *J. Physiol. (Lond.)* **562**, 785-799, doi:10.1113/jphysiol.2004.079228 (2005).

32 Ma, M. Multiple Olfactory Subsystems Convey Various Sensory Signals. BTI - The Neurobiology of Olfaction.

33 Lin, W., Ezekwe, E. A. D., Zhao, Z., Liman, E. R. & Restrepo, D. TRPM5-expressing microvillous cells in the main olfactory epithelium. *BMC neuroscience* **9**, 114, doi:10.1186/1471-2202-9-114 (2008).

34 Lin, W., Ogura, T., Margolskee, R. F., Finger, T. E. & Restrepo, D. TRPM5-expressing solitary chemosensory cells respond to odorous irritants. *Journal of Neurophysiology* **99**, 1451-1460, doi:10.1152/jn.01195.2007 (2008).

35 Choi, R. & Goldstein, B. J. Olfactory epithelium: Cells, clinical disorders, and insights from an adult stem cell niche. *Laryngoscope Investig Otolaryngol* **3**, 35-42, doi:10.1002/lio2.135 (2018).

36 Schwob, J. E. *et al.* Stem and progenitor cells of the mammalian olfactory epithelium: Taking poietic license. *J. Comp. Neurol.* **525**, 1034-1054, doi:10.1002/cne.24105 (2017).

37 Fletcher, R. B. *et al.* Deconstructing Olfactory Stem Cell Trajectories at Single-Cell Resolution. *Cell Stem Cell* **20**, 817-830.e818, doi:10.1016/j.stem.2017.04.003 (2017).

38 Hoffmann, M. *et al.* SARS-CoV-2 Cell Entry Depends on ACE2 and TMPRSS2 and Is Blocked by a Clinically Proven Protease Inhibitor. *Cell*, doi:10.1016/j.cell.2020.02.052 (2020).

39 Li, W. *et al.* Angiotensin-converting enzyme 2 is a functional receptor for the SARS coronavirus. *Nature* **426**, 450-454, doi:10.1038/nature02145 (2003).

40 Netland, J., Meyerholz, D. K., Moore, S., Cassell, M. & Perlman, S. Severe acute respiratory syndrome coronavirus infection causes neuronal death in the absence of encephalitis in mice transgenic for human ACE2. *J. Virol.* **82**, 7264-7275, doi:10.1128/JVI.00737-08 (2008).

41 Li, W. *et al.* Efficient replication of severe acute respiratory syndrome coronavirus in mouse cells is limited by murine angiotensin-converting enzyme 2. *J. Virol.* **78**, 11429-11433, doi:10.1128/JVI.78.20.11429-11433.2004 (2004).

42 Kuba, K. *et al.* A crucial role of angiotensin converting enzyme 2 (ACE2) in SARS coronavirus-induced lung injury. *Nat. Med.* **11**, 875-879, doi:10.1038/nm1267 (2005).

43 Bertram, S. *et al.* Influenza and SARS-coronavirus activating proteases TMPRSS2 and HAT are expressed at multiple sites in human respiratory and gastrointestinal tracts. *PLoS ONE* **7**, e35876, doi:10.1371/journal.pone.0035876 (2012).

44 Bertram, S. *et al.* Cleavage and activation of the severe acute respiratory syndrome coronavirus spike protein by human airway trypsin-like protease. *J. Virol.* **85**, 13363-13372, doi:10.1128/JVI.05300-11 (2011).

45 Sungnak, W., Huang, N., Bécavin, C., Berg, M. & Network, H. C. A. L. B. SARS-CoV-2 Entry Genes Are Most Highly Expressed in Nasal Goblet and Ciliated Cells within Human Airways. doi:papers3://publication/uuid/3C4FCA0A-9DA2-4431-B59C-5B1A38C2E1F2 (2020).

46 Deprez, M. *et al.* A single-cell atlas of the human healthy airways. *bioRxiv* **24**, 3000-3049, doi:10.1101/2019.12.21.884759 (2019).

47 Vieira Braga, F. A. *et al.* A cellular census of human lungs identifies novel cell states in health and in asthma. *Nat. Med.* **25**, 1153-1163, doi:10.1038/s41591-019-0468-5 (2019).

48 Durante, M. A. *et al.* Single-cell analysis of olfactory neurogenesis and differentiation in adult humans. *Nature Publishing Group* **23**, 323-326, doi:10.1038/s41593-020-0587-9 (2020).

49 Gadye, L. *et al.* Injury Activates Transient Olfactory Stem Cell States with Diverse Lineage Capacities. *Cell Stem Cell* **21**, 775-790.e779, doi:10.1016/j.stem.2017.10.014 (2017).

50 Wu, Y. *et al.* A Population of Navigator Neurons Is Essential for Olfactory Map Formation during the Critical Period. *Neuron* **100**, 1066-1082.e1066, doi:10.1016/j.neuron.2018.09.051 (2018).

51 Colquitt, Bradley M., Markenscoff-Papadimitriou, E., Duffié, R. & Lomvardas, S. Dnmt3a Regulates Global Gene Expression in Olfactory Sensory Neurons and Enables Odorant-Induced Transcription. *Neuron* **83**, 823-838, doi:10.1016/j.neuron.2014.07.013 (2014).

52 Saraiva, L. R. *et al.* Hierarchical deconstruction of mouse olfactory sensory neurons: from whole mucosa to single-cell RNA-seq. *Sci Rep* **5**, 18178, doi:10.1038/srep18178 (2015).

53 Kanageswaran, N. *et al.* Deep Sequencing of the Murine Olfactory Receptor Neuron Transcriptome. *PLOS ONE* **10**, e0113170, doi:10.1371/journal.pone.0113170 (2015).

54 Saraiva, L. R. *et al.* A transcriptomic atlas of mammalian olfactory mucosae reveals an evolutionary influence on food odor detection in humans. *Science Advances* **5**, eaax0396, doi:10.1126/sciadv.aax0396 (2019).

55 Olender, T. *et al.* The human olfactory transcriptome. *BMC Genomics* **17**, 619, doi:10.1186/s12864-016-2960-3 (2016).

56 Plasschaert, L. W. *et al.* A single-cell atlas of the airway epithelium reveals the CFTR-rich pulmonary ionocyte. *Nature* **560**, 377-381, doi:10.1038/s41586-018-0394-6 (2018).

57 Weng, P.-L., Vinjamuri, M. & Ovitt, C. E. Ascl3 transcription factor marks a distinct progenitor lineage for non-neuronal support cells in the olfactory epithelium. *Sci Rep* **6**, 38199-38111, doi:10.1038/srep38199 (2016).

58 Bihun, C. G. & Percy, D. H. Morphologic changes in the nasal cavity associated with sialodacryoadenitis virus infection in the Wistar rat. *Vet. Pathol.* **32**, 1-10, doi:10.1177/030098589503200101 (1995).

59 Youngentob, S. L., Schwob, J. E., Saha, S., Manglapus, G. & Jubelt, B. Functional consequences following infection of the olfactory system by intranasal infusion of the olfactory bulb line variant (OBLV) of mouse hepatitis strain JHM. *Chemical Senses* **26**, 953-963, doi:10.1093/chemse/26.8.953 (2001).

60 Dubé, M. *et al.* Axonal Transport Enables Neuron-to-Neuron Propagation of Human Coronavirus OC43. *J. Virol.* **92**, doi:10.1128/JVI.00404-18 (2018).

61 Schwob, J. E., Saha, S., Youngentob, S. L. & Jubelt, B. Intranasal inoculation with the olfactory bulb line variant of mouse hepatitis virus causes extensive destruction of the olfactory bulb and accelerated turnover of neurons in the olfactory epithelium of mice. *Chemical Senses* **26**, 937-952, doi:10.1093/chemse/26.8.937 (2001).

62 Farbman, A. I. Olfactory neurogenesis: genetic or environmental controls? *Trends Neurosci* **13**, 362-365, doi:10.1016/0166-2236(90)90017-5 (1990).

63 Sultan-Styne, K. *et al.* Long-term survival of olfactory sensory neurons after target depletion. *J. Comp. Neurol.* **515**, 696-710, doi:10.1002/cne.22084 (2009).

64 Lin, B. *et al.* Injury Induces Endogenous Reprogramming and Dedifferentiation of Neuronal Progenitors to Multipotency. *Cell Stem Cell* **21**, 761-774.e765, doi:10.1016/j.stem.2017.09.008 (2017).

65 Eriksson, C. & Brittebo, E. B. Dichlobenil in the fetal and neonatal mouse olfactory mucosa. *Toxicology* **96**, 93-104, doi:10.1016/0300-483x(94)02914-g (1995).

66 Krolewski, R. C., Packard, A. & Schwob, J. E. Global expression profiling of globose basal cells and neurogenic progression within the olfactory epithelium. *J. Comp. Neurol.* **521**, 833-859, doi:10.1002/cne.23204 (2013).

67 Bohmwald, K., Gálvez, N. M. S., Ríos, M. & Kalergis, A. M. Neurologic Alterations Due to Respiratory Virus Infections. *Front Cell Neurosci* **12**, 386, doi:10.3389/fncel.2018.00386 (2018).

68 Barnett, E. M. & Perlman, S. The olfactory nerve and not the trigeminal nerve is the major site of CNS entry for mouse hepatitis virus, strain JHM. *Virology* **194**, 185-191, doi:10.1006/viro.1993.1248 (1993).

69 Wheeler, D. L., Athmer, J., Meyerholz, D. K. & Perlman, S. Murine Olfactory Bulb Interneurons Survive Infection with a Neurotropic Coronavirus. *J. Virol.* **91**, doi:10.1128/JVI.01099-17 (2017).

70 Li, Y. C., Bai, W. Z. & Hashikawa, T. The neuroinvasive potential of SARS-CoV2 may play a role in the respiratory failure of COVID-19 patients. *J. Med. Virol.*, doi:10.1002/jmv.25728 (2020).

71 Hemmila, E. *et al.* Ceacam1a-/- mice are completely resistant to infection by murine coronavirus mouse hepatitis virus A59. *J. Virol.* **78**, 10156-10165, doi:10.1128/JVI.78.18.10156-10165.2004 (2004).

72 Weinreb, C., Wolock, S. & Klein, A. M. SPRING: a kinetic interface for visualizing high dimensional single-cell expression data. *Bioinformatics* **34**, 1246-1248, doi:10.1093/bioinformatics/btx792 (2018).

73 Wolock, S. L., Lopez, R. & Klein, A. M. Scrublet: Computational Identification of Cell Doublets in Single-Cell Transcriptomic Data. *Cell Systems* **8**, 281-291.e289, doi:10.1016/j.cels.2018.11.005 (2019).

74 Weinreb, C., Rodriguez-Fraticelli, A., Camargo, F. D. & Klein, A. M. Lineage tracing on transcriptional landscapes links state to fate during differentiation. *Science* **367**, eaaw3381, doi:10.1126/science.aaw3381 (2020).

75 Polański, K. *et al.* BBKNN: fast batch alignment of single cell transcriptomes. *Bioinformatics* **36**, 964-965, doi:10.1093/bioinformatics/btz625 (2019).